Electronic consequences of lateral composition modulation in semiconductor alloys

T. Mattila, L.-W. Wang, and Alex Zunger*
National Renewable Energy Laboratory, Golden, Colorado 80401
(Received 16 November 1998)

where A is the amplitude, λ is the wavelength and $\vec{u}$ is a vector along the direction of the modulation. For III-V semiconductor alloys, $\lambda \approx 100-200$ Å, and $A \approx 1-20\%$, depending on growth conditions.[5,6,8–13] The function $f_{\lambda,\vec{u}}$ is a rounded square wave or sinusoidal, e.g., $f_{\lambda,\vec{u}}(\vec{R}) = \sin[(2\pi\vec{R}\cdot\vec{u}/\lambda)]$. In most of the experimentally studied systems $\vec{u}$ is along $[\bar{1}10]$ or $[110]$.[5,6,8–13]

Figure 1 illustrates, for InAs/GaAs, the structures of (a) lateral [110] alloy CM of $In_xGa_{1-x}As$ without any superlattice (SL) structure [Eq. (1)], (b) pure [001] SL, and (c) a combination of both. The atomic positions were calculated by minimizing the strain energy, as explained in Sec. II A. In the [001] superlattice [Fig. 1(b)] the atomic layer sequence consists of two InAs monolayers followed by two monolayers of GaAs. We see that a combination of [001] SL with [110] oriented lateral CM [Fig. 1(a)] results [Fig. 1(c)] in the wirelike structure. Experimental studies have shown that the strongest lateral CM is observed when the deposited superlattice layers have *noninteger* values, i.e., for $(AC)_n/(BC)_m$ superlattice $(n,m \neq$

There are three previous attempts at modeling the electronic structure of CM 1 SL systems: by Mascarenhas *et al.*,[8] by Rich *et al.*,[7] and by Zhang and Mascarenhas.[22] We have recently presented[23] an *atomistic* study of CM 1 SL. There are several reasons why atomistic study is needed here: (1) The problem involves a substitutional alloy, which cannot be described accurately by continuum models, especially when composition fluctuations[24] or ordering exist. (2) Short-period ($n \sim 2$) SL exists in the system. It has been shown[25] that the continuum effective mass or **k•p** model cannot be used to describe the electronic structure of a short-period SL. (3) Microscopic strain plays an important part in the problem. As will be shown below (Sec. III B) the continuum models are not able to describe the microscopic strain accurately. However, a large system size ($\sim 10^4$ atoms) is required in the atomistic approach, since the cell has to incorporate one complete CM wavelength ($\lambda \sim 100$F 8

Problem (2) will be addressed by using specially constructed atomic pseudopotentials which have explicit dependence on the local strain. These pseudopotentials are fitted to reproduce bulk band structures, hydrostatic and biaxial deformation potentials, and natural and biaxially strained band offsets based on available experimental and theoretical (first-principles local-density approximation method) data. Thus, the coupling of atomic displacements to the electronic structure is described atomically and explicitly. In earlier studies[8,7,22] the atomic degrees of freedom were coupled to electronic structure rather approximately using a continuum strain-dependent $\mathbf{k}\cdot\mathbf{p}$ Hamiltonian. This has resulted in some ambiguity in the band alignment in CM systems: the studies by Mascarenhas *et al.*[8] and Tang *et al.*[7] model CM in $Ga_{1-x}In_xP$ as a piecewise constant effective-mass superlattice and find a type-II alignment between Ga-rich and In-rich regions. This led to the prediction that CM in $Ga_{1-x}In_xP$ will spatially separate electrons and holes, and to the proposal of a new solar cell device structure based on this effect[27]. In the more recent study, Zhang and Mascarenhas[22] used a multiband $\mathbf{k}\cdot\mathbf{p}$ method with spatially varying effective potential. They find this time a type-I alignment with no electron-hole separation for all CM systems ($Ga_{1-x}In_xP$, $Ga_{1-x}In_xAs$, $Al_xIn_{1-x}As$) covered in their study. It would be desirable to determine more rigorously whether or not CM leads to electron-hole separation.

Problem (3) will be solved by a general expansion of the wave function in plane waves and a direct diagonalization of the pseudopotential Hamiltonian in this basis. Thus, the effects of the SL of CM are included directly, no effective-mass approximation is used (particularly questionable for short-period, 1–2 monolayer, superlattices[25]) and a multiband coupling is allowed. Previous studies of CM (Refs. 8,7 and 22) have relied on their approach on the effective-mass theory. Mascarenhas *et al.*[8] and Tang *et al.*[7] ignored the potential-energy modulation along the CM direction, and included a kinetic-energy modulation via variation of the effective mass. Furthermore, the SL was not considered directly; its effect was included indirectly and partially by including a crystal-field splitting for the pseudo-alloy describing the SL. Ref. 22 included the SL via the anticipated crystal-field splitting it causes, but ignored the electronic structure of the SL (e.g., the $\Gamma-X$ coupling it causes) or the Hamiltonian coupling of the SL with the CM.

Our main results are:

(i) CM in GaP/InP and GaAs/InAs shows type-I band alignment (electrons and holes localized in the same spatial region). Inclusion of a vertical SL does not alter the band alignment. We use AlP/GaP as an example of a system exhibiting a type-II alignment.

(ii) Both CM and SL induce significant band gap redshifts with respect to the random alloy. In a combined CM+SL system their contributions add up nearly linearly: for $A=8\%$ we find $\Delta E_{gap}=-40(-215)$ meV in $Ga_{1-x}In_xAs$ ($Ga_{1-x}In_xP$), of which the SL contribution is $\sim-20(-130)$ meV.

(iii) The lowest energy transitions between the conduction and valence states are distinctly polarized due to CM and SL: the transitions polarized along the composition wave (lateral for CM and vertical for SL) are surpressed by being shifted to higher energy. In the combined CM+SL system CM and SL act as sequential filters. The CM+SL system in $Al_xGa_{1-x}P$ is found to have an indirect band gap (in reciprocal space), limiting its use in practical optical applications.

This study thus shows that if one were able to control growth parameters to select desirable CM amplitude (A) and wavelength (λ) it would be possible to tailor the optical properties of semiconductor alloys in a significant way.

II. METHOD OF CALCULATION

We wish to solve the Schrödinger equation

$$\left\{-\frac{1}{2}\nabla^2+\sum_{\alpha,m} v_\alpha(\mathbf{r}-\mathbf{R}_{\alpha,m})\right\}\psi_i(\mathbf{r})=\epsilon_i\psi_i(\mathbf{r}), \qquad (2)$$

the system is deformed with respect to the ideal structure. For example, the individual band-edge deformation potentials a_{CBM} and a_{VBM} and band offsets in lattice-mismatched systems are difficult to fit correctly even qualitatively. This is because the pseudopotential form $v_\alpha(q,0)$ does not contain any dependence on the local atomic environment which would describe the change in the potential due to deformation. This shortcoming of $v_\alpha(q,0)$ does not appear in self-consistently screened potentials since the latter builds in the effect of charge redistribution due to the deformation. The form $v_\alpha(q,\mathcal{E})$ supplies this needed dependence of the potential on its atomic environment. For cubic materials, we model the pseudopotential dependence on $\mathcal{E}$ by using the trace of the strain tensor $[\mathrm{Tr}(\mathcal{E})]$ to describe the changes in the local atomic environment. The functional form chosen for $v_\alpha(q,0)$ is

$$v_\alpha(\mathbf{q},\mathcal{E}) = a_{0\alpha}\frac{(q^2 - a_{1\alpha})}{a_{2\alpha}e^{a_{3\alpha}q^2} - 1}[1 + a_{4\alpha}\mathrm{Tr}(\mathcal{E})], \tag{4}$$

where $a_{i\alpha}$ $i=0,1,2,3,4$ are the parameters to be fitted.

The functional form is chosen to give sufficient flexibility to describe as many physical quantities as possible without ''overfitting'' the potential by including too many parameters. It also provides a functional form that resembles the final form from the outset and will therefore only require some small optimization for each atomic type rather than dramatic changes, thus stabilizing the optimization process.

These types of pseudopotentials have been shown to produce reliable results for lattice-mismatched III-V systems where the strain dependence plays a crucial role: random alloys, strained superlattices, and embedded quantum dots.[31,32]

The pseudopotential fits and the parameters $a_{i\alpha}$ employed in this study for GaAs, InAs, AlP, GaP, and InP are listed in the Appendix. A 5 Ry kinetic-energy cutoff was used when generating the pseudopotentials. To avoid discontinuities in the calculated band structure, a smoothing function was applied near the cutoff energy E_{cut}.[33] The Appendix compares the EPM calculated band-edge energies at high symmetry points, electron and heavy-hole effective masses, hydrostatic and biaxial deformation potentials with the first-principles and experimental values used as a reference in the fitting procedure. The Appendix further shows the natural and strained valence band offsets given by the applied pseudopotentials and makes comparison with the reference values. The Appendix also gives the band-gap redshifts in CuPt ([111]-oriented SL with period $n=1$) and Z2 ([001]-oriented SL with period $n=2$) *alloy* structures with respect to random alloy. In general, we see that the generated pseudopotentials reproduce well the reference values.

In the alloy environment we have used a weighted average for the anion pseudopotentials based on the local atomic configuration surrounding an anion site. For example, in $\mathrm{Ga}_{1-x}\mathrm{In}_x\mathrm{As}$, there are two pseudopotentials $v_{\mathrm{As(Ga)}}$ and $v_{\mathrm{As(In)}}$ resulting from the fits performed for binary GaAs and InAs. The pseudopotential used at an As atomic site is

$$v_{\mathrm{As}} = \frac{n_{\mathrm{Ga}}}{4}v_{\mathrm{As(Ga)}} + \frac{n_{\mathrm{In}}}{4}v_{\mathrm{As(In)}}, \tag{5}$$

where $n_{\mathrm{Ga(In)}}$ denote how many of the four nearest-neighbor cations surrounding the As site are Ga (In) atoms, respectively. We emphasize that, although this weighted average of pseudopotentials in the *anion* sublattice *locally* resembles the spirit of virtual crystal approximation (VCA), the description of the full alloy (mixed *cation* sublattice) is based on explicit treatment of individual atoms rather than VCA.

In order to check the effect of spin-orbit (SO) splitting in the CM systems, we have constructed a set of pseudopotentials for GaAs and InAs including the SO effects. We use the same functional form as in Eq. (3), and include the SO interaction by introducing a nonlocal term.[33] This nonlocal potential is represented by a Kleinman-Bylander separable form in real space, which allows order-*N* scaling for calculations with large system size.[32] The resulting pseudopotentials are listed in the Appendix which also compares the SO pseudopotential (SO–EPM) with the pseudopotential omitting SO effects (NSO–EPM), and the reference experimental and first-principles values. The accuracy of the SO–EPM can be seen to be similar to the NSO–EPM.

C. Solving the Schrödinger equation

The realistic modeling of a CM system requires the use of supercells containing typically $\sim 30\,000$ atoms. This sets special requirements for solving the electronic structure.

To expand the electronic wave functions, we use the plane-wave basis:

$$\psi_i = \sum_{\mathbf{G}} c_{\mathbf{k}+\mathbf{G}} e^{i\mathbf{k}+\mathbf{G}\cdot\mathbf{r}}, \tag{6}$$

where $\mathbf{G}$ runs over the reciprocal lattice lattice vectors fulfilling the kinetic-energy cutoff $(\frac{1}{2}|\mathbf{k}+\mathbf{G}|^2 < 5\mathrm{Ry})$. Using this expansion for wave functions we calculate the eigenstates of the Schrödinger equation [Eq. (2)] using the folded spectrum method (FSM),[34] where one solves

$$(H - \epsilon_{\mathrm{ref}})^2\psi_i$$

A. Construction of the composition modulation supercell

We first consider sinusoidal composition modulation in $Ga_{1-x}In_xAs$ at $x_0 = 0.5$ and $\hat{k}$ along a [110] direction using Eq. (1). We construct a periodic ''supercell'' containing a full period of $x(R)$ of Eq. (1) by stacking along the $\hat{k}$ direction n planes with lattice vectors perpendicular to the modulation $a_1 = N(\bar{1},1,0)\,a_0$, and $a_2 = N(0,0,1)a_0$, where a_0 is the cubic lattice constant of $Ga_{0.5}In_{0.5}As$ and N is an integer driving the lengths of the in-plane lattice vectors. For $N = 10$, we have 200 cations and 200 anions per plane. The number of planes is $n \approx (4/\sqrt{2})(\lambda/a_0)$. For example, for $\lambda = 150$ Å we have $n = 72$, leading to a number of atoms (anions and cations) in the supercell of $4N^2 n = 28\,800$. In each plane we occupy the 2 N^2 cation-lattice sites randomly[35], so as to produce a plane composition given by $x(R)$. Figure 3(a) shows our composition profile $x(R)$ along the $\hat{k} = [110]$ direction with modulation amplitude $A = 8\%$.

B. Atomic relaxation and strain fields

Having constructed a periodic composition wave, we now permit all atoms in the supercell to relax away from their nominal zinc-blende sites so as to minimize the elastic VFF strain energy. No symmetry constraints are assumed, i.e., the atomic relaxation is not restricted to the modulation direction. We find that the main relaxation occurs in the [110] CM direction in the supercell: for the (110) planes in the Ga-rich (In-rich) region the interplanar spacing contracts (expands). To illustrate this, Fig. 3(b) shows the [110] strain component induced by pure CM. We note that the strain wave [Fig. 3(b)] is commensurate with the composition wave [Fig. 3(a)]. The solid line in Fig. 3(b) corresponds to the strain calculated directly using the VFF method, i.e., atomic elasticity. This strain is used throughout this work. The strain along the [110] direction is calculated by averaging over the atomic local strains in each (110) plane. The dashed line in the same figure shows the [110] strain calculated using continuum elasticity. Assuming the cartesian coordinate system x, y and z corresponding to [100], [010] and [001] directions, the continuum elasticity tetragonal strain along the [110] direction can be evaluated as[22]

$$\mathcal{E}_{[110]} = \mathcal{E}_{xx} + \mathcal{E}_{xy} = \mathcal{E}_{zz}\frac{2c_{44} - c_{11} - 3c_{12}}{2c}$$

subsection how coupling of the strain with the composition wave is going to modify the energy levels relative to the random alloy. To study the *qualitative* physics we wish to consider the CBM and VBM energies along the [110] CM composition wave. In order to simply mimic the local atomic environment along the composition wave, we construct smaller [110]-oriented supercells.[36] We occupy the cation sublattice randomly in these cells so that the composition corresponds to $x(\vec{R})$. To imitate the average strain along the [110] direction in the large CM supercell [Fig. 3(b)], the shape of the small supercell is chosen in the following way: The supercell vector lengths along $[\bar{1}10]$ and [001] correspond to the lattice constant of the $x=0.50$ alloy given by Vegard's rule, while the length of the [110] cell vector is adjusted for each $x(\vec{R})$ to give the strain along [110] illustrated in Fig. 3(b). Full relaxation of the atoms in the small supercell is then performed using the VFF method, and the eigenstates of the Hamiltonian (without spin-orbit interaction) are consequently solved using the same method (atomic pseudopotentials, folded-spectrum method) as used for the large CM cell as reported in our full numerical calculation in Sec. III D.

The resulting band-edge energies are shown in Figs. 3(c) and 3(d). Figure 3

(up). Thus, the band gap widens (narrows) in the Ga-rich (In-rich) region, as expected from the larger band gap for GaAs than for InAs. The strain effect has qualitatively the same contribution as the alloy effect for CBM and the two uppermost valence states. For the third valence state (V_c), however, the strain has an opposite effect: due to strain V_c has its maximum in the Ga-rich region while V_a and V_b have their maxima in the In-rich region. Based on this decomposition analysis into alloy and strain contributions it is evident that an accurate description of both compositional and strain effects is essential for a realistic modeling of the band-edge states in a CM system.

D. Band-gap redshift

As the modeled band edges show in Figs. 3(c) and 3(d), the smallest band gap occurs in the In-rich region of the CM system. Combined with the information that the CBM and VBM are localized in the In-rich region [Figs. 3(e) and 3(f)] the CM is expected to induce band-gap narrowing (redshift) with respect to a random alloy. While Figs. 3(c) and 3(d) were the result of a simple model (Sec. III C), we now use direct diagonalization to solve Eq. (2) for the full 28 800 atom minimum strain configuration. The result is given in Fig. 5 which shows the behavior of CBM and uppermost VB states as a function of the CM amplitude A(A 5 0 corresponds to a fully random system). We indeed see that CM shifts VBM up while CBM drops, the combined effect being a band-gap redshift which is about 40 meV for 10% modulation amplitude.

We have also made calculations where the composition profile f is changed from a sinusoidal to a steplike function. We see that the band-gap redshift increases slightly, for A 5 8% the increase is ~5 meV. Also, we have investigated the effect of varying the modulation wavelength λ. We find that the behavior of the band-edge states and band gap is rather insensitive to λ: the band gap increases linearly by ~5 meV when λ is varied from 116 Å to 182 Å.

E. Polarization of optical transitions

In order to analyze the polarization of the lowest energy optical transitions, we have calculated the dipole matrix elements between the lowest conduction state and the valence states

p_α

tion). The transition from CBM to V_3 is [001] polarized while the transition from CBM to V_4 is [110] polarized.

IV. COMBINATION OF LATERAL COMPOSITION MODULATION AND VERTICAL SHORT-PERIOD SUPERLATTICE

Having illustrated the physics induced by a pure lateral CM in Sec. III, we now turn to modeling the combined system of lateral CM and vertical SL which corresponds to the actual experimental case.

A. Structure: Integer vs. fractional period superlattice GaAs/InAs

Experimental studies[9,11–13] show that the strongest lateral CM is observed when superlattice layers have *noninteger* values, i.e., for $(\mathrm{AC})_n/(\mathrm{BC})_m$ superlattice $(n,m \neq 1,2,\ldots)$. To gain insight into the role of the superlattice period, we investigate the two structures illustrated in Figs. 1 and 2. The atomic positions shown correspond to minimum strain configuration, the atomic strain being calculated as described in Sec. II A. The crucial difference between Figs. 1 and 2 is the superlattice period: Fig. 1(b) shows *integer* $(n5 2)$ period

The main effect of the spin-orbit interaction in the binary GaAs or InAs system is that it splits the otherwise triply degenerate VBM Γ_{15v} into two components: doubly degenerate Γ_{8v}, and a split-off state Γ_{7v}, 0.34 (0.38) eV lower in energy in GaAs (InAs). The question we want to ask is: does this affect the delicate VBM structure in CM 1 SL structure and if so, how? Comparison between panels (a) and (b) of Fig. 8 corresponding to calculations excluding and including the spin-orbit effects reveals only minor differences: the CBM and the two uppermost valence states exhibit the same character, while small differences are visible in the order of the lower valence band states. We thus conclude that, surprisingly, the spin-orbit interaction does not play a dominant role in determining the behavior of the band-edge states in the CM 1 SL systems.

The wave function densities shown for the $Ga_{12x}In_xP$ CM 1 SL system in Fig. 8(c) show that $Ga_{12x}In_xP$ also exhibits type-I band alignment. In Fig. 9 we use $Al_xGa_{12x}P$ as an example to demonstrate type-II band alignment in the [110] CM 1 [001] SL (n 5 1.5) system. It is immediately evident that CBM and VBM wave functions are localized in different regions. This is a direct consequence of the type-II natural (unstrained) band offset between AlP and GaP: the VBM (CBM) of GaP resides 0.54 (0.58) eV lower than in AlP. Thus, it is possible to generate a type-II CM if one uses constituents that already have a type-II alignment. This phenomenon could be used, e.g., in reducing the electron-hole recombination in a solar-cell structure as proposed by Mascarenhas *et al.*[27] However, $Al_xGa_{12x}P$ alloy seems not to be a good candidate for this application due to inefficient light absorption induced by the indirect band gap (see Sec. IV E).

D. Band-gap redshift: GaAs/InAs, AlAs/InAs, GaP/InP

Figure 10 shows the behavior of the band edges and band gap as a function of the modulation amplitude A for the combined [110] CM and [001] SL (n 5 1.5) structure. Panel (a) also shows the band-gap reduction for the system with [110] CM 1 [001] n 5 2.0 SL and pure [110] CM. The data points at A 5 0.0 correspond to pure SL without CM. We see that the pure [001] SL induces a significant redshift which mainly originates from downshift in CBM. The contribution to the redshift from fractional (n 5 1.5) and integer (n 5 2) period superlattices is nearly the same. Panel (a) reveals also that the redshift induced by the CM 1 SL system is nearly a linear combination of the pure CM and SL contributions.

Figure 11 compares the shift in the band-edge states and band gap between the $Ga_{12x}In_xAs$ and $Ga_{12x}In_xP$ CM 1 SL systems. We see that the CM 1 SL induced band-gap redshift is much larger in $Ga_{12x}In_xP$ than in $Ga_{12x}In_xAs$. This is induced by two factors:

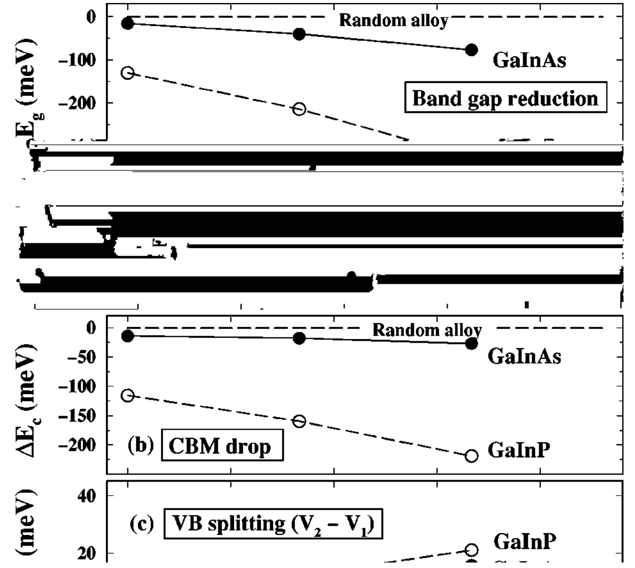

FIG. 11. The comparison of the band-gap and the band-edge states in Ga$_{1-x}$In$_x$As and Ga$_{1-x}$In$_x$P systems exhibiting both [110] composition modulation and [001] superlattice ($n=1.5$) as a function of sinusoidal composition modulation amplitude A. The modulation wavelength λ is 149 Å for Ga$_{1-x}$In

band alignment between the binary materials: (i) the valence band offset between GaP and InP (0.11 eV) is about twice the value for GaAs/InAs (0.057 eV), (ii) the conduction band offset, calculated at Γ point which is relevant for the alloy comparison, is significantly larger (1.30 eV) for GaP/InP than for GaAs/InAs (1.04 eV). The conduction band offsets are thus much larger than valence band offsets; Fig. 11(b) reveals that the drop in the conduction band minimum indeed constitutes most of the band-gap redshift in both materials. Figure 11(c) shows that the energy difference between the two highest valence band states increases nearly linearly from a few meV to ~15 meV as a function of modulation amplitude A in both Ga$_{1-x}$In$_x$As and Ga$_{1-x}$In$_x$P.

The calculated band-gap redshifts are in good agreement with available experimental data. In Ga$_{1-x}$In$_x$As the reported values are in the range from a few tens of meV up to ~100.[11] In Ga$_{1-x}$In$_x$P the reported values are typically significantly larger (~250 meV).[5,6,8]

E. Polarization of optical transitions

Figure 12 illustrates the polarizations calculated for the lowest energy transitions in pure [110] CM, pure [001] SL (n5 1.5), and [110] CM 1 [001] SL systems.

We find that the lateral CM and vertical SL act as sequential filters. (i) Similar to Fig. 6, in the pure [110] CM the

TABLE VI. The pseudopotential fit for InP.

Properties	NSO-EPM	LAPW	Expt.
Γ_{1c}	1.45		1.46[a]
X_{5v}	−1.95		−2.20[b]
X_{1c}	2.25		2.38[a,c]
L_{3v}	−0.78		−1.23[d]
L_{1c}	1.94		2.03[e,a]
m_e	0.088		0.077[f]
$m_{hh}(100)$	0.46		0.56[g]
$a_g(\Gamma)$	−6.84	−5.18	−6.4[h]
$a_v(\Gamma)$	−0.49	−0.41	
b	−1.71	−1.97	−2.0[a]

[a]Reference 58.
[b]Reference 59.
[c]Reference 60.
[d]Reference 61.
[e]Reference 62.
[f]Reference 63.
[g]Reference 64.
[h]Reference 44.

We have also analyzed the transition probabilities for the $Al_xGa_{1-x}P$ CM+SL system exhibiting type-II band alignment (Fig. 9). The full transition probabilities from the CBM to the four uppermost valence states are extremely small due to the lack of spatial overlap in the conduction and valence band wave functions. Type-II band alignment is present also in reciprocal space: decomposition of the CBM into Bloch states with k-vector sampling in the principal directions in the first Brilloun zone, reveals that it has very little Γ character, while VBM is principally Γ-like. This is an obvious consequence of both AlP and GaP binaries having an indirect gaps in reciprocal space. In fact, we find that already the pure $n=1.5$ SL is indirect system in reciprocal space.

TABLE VII. Calculated valence band offsets of AC/BC, strained on a substrate lattice constant $a_{\parallel}$ in the {001} plane. For the strained material (**boldfaces**) the lattice constant along the [001] direction ($a_{\perp}$) is fully relaxed by using the valence force field approach. a^* denotes *natural* unstrained valence band offsets, i.e., $E_{\rm VBM}^{\rm AC}(a_{\rm AC})-E_{\rm VBM}^{\rm BC}(a_{\rm BC})$. A positive offset means that the VBM energy of the material AC in AC/BC is above that of BC.

AC/BC	$a_{\parallel}$	LAPW offset (eV)	NSO–EPM offset (eV)	SO–EPM offset (eV)
InAs/GaAs	a^*	0.057	0.056	0.045
InAs/GaAs	$a_{\rm GaAs}$	0.38	0.40	0.42
InAs/**GaAs**	$a_{\rm InAs}$	−0.25	−0.22	−0.39
GaP/AlP	a^*	0.54	0.54	
InAs/AlAs	a^*	0.58	0.56	
InAs/AlAs	$a_{\rm AlAs}$	0.89	0.91	
InAs/**AlAs**	$a_{\rm InAs}$	0.13	0.13	
InP/GaP	a^*	0.11	0.09	
InP/GaP	$a_{\rm GaP}$	0.43	0.43	
InP/**GaP**	$a_{\rm InP}$	−0.32	−0.25	

TABLE VIII. Calculated band-gap redshifts ΔE_g with respect to random alloy in CuPt ([111]-oriented SL with period $n=1$) and $Z2$ ([001]-oriented SL with period $n=2$) structures.

		ΔE_g NSO–EPM (eV)	ΔE_g LAPW (eV)
GaAs/InAs	CuPt	−0.05	−0.25
	$Z2$	−0.02	−0.05
GaP/InP	CuPt	−0.34	−0.42
	$Z2$	−0.12	−0.11

V. SUMMARY AND CONCLUSIONS

We apply (i) atomistic description for strain as calculated with a valence force field approach, (ii) specially constructed strain-dependent empirical pseudopotentials, and (iii) plane-wave basis for the expansion of electronic wave functions to resolve the atomic and electronic structure resulting from lateral composition modulation in vertical short-period superlattices. Detailed analysis of a pure CM wave in $Ga_{1-x}In_xAs$ alloy shows that a careful consideration of both strain and alloy composition effects are necessary for a realistic description of the CM system. This fact is emphasized in the combined CM+SL system where the orthogonal strain fields, induced by CM and SL composition waves with different characteristic lengths, interact in a complex manner.

We show that for GaAs/InAs and GaP/InP systems, the electron-hole localization in type-I, i.e., the natural band alignment between the binaries, persists in the CM+SL system. Similarly for AlP/GaP systems, exhibiting type-II alignment between the binary compounds, we find type-II alignment also in the CM+SL system. Both CM and SL are found to contribute significantly to the behavior of band-edge states in CM+SL system:

(i) Both CM and SL induce band-gap narrowing with respect to random alloy, the main contribution originating from a drop in conduction band energy. The GaP/InP system is found to exhibit significantly larger band-gap reduction than GaAs/InAs. This is a consequence of the larger natural conduction and valence band offsets between GaP and InP than between GaAs and InAs.

(ii) The symmetry of the uppermost valence band states is strongly influenced by both CM and SL. As a consequence, the lowest energy optical transitions between conduction and valence band exhibit polarization: the component perpendicular to the CM wave has the lowest energy and highest transition probability, and the component parallel to the CM wave is suppressed by a shift to higher energy. The strong polarization dependence is in agreement with experimental observations.

TABLE IX. Screened atomic pseudopotential parameters for the arsenide semiconductors *excluding* the spin-orbit interaction. The a parameters refer to Eq. (4). A 5 Ry cutoff was used in the fitting.

	a_0	a_1	a_2	a_3	a_4
Ga	55 738.5	2.793	3209.4	0.283	1.862
In	107.755	1.915	3.460	0.414	1.665
As(GaAs)	48.54	2.536	1.463	0.494	0.000
As(InAs)	49.614	2.737	1.523	0.574	0.000

In AlP/GaP CM 1 SL systems the optical transition probabilities are small due to an indirect band gap, which makes the practical exploitation of the type-II band alignment difficult, e.g., in solar-cell applications.

In general, our results thus show that if the control in growth parameters to select desirable CM amplitude (A) and wavelength (λ) etc., was achieved, the optical properties of semiconductor alloys could be tailored.

ACKNOWLEDGMENTS

We thank S.-H. Wei for providing the LAPW values employed in pseudopotential fits. T. M. acknowledges the financial support by the Väisälä Foundation (Helsinki, Finland). This work was supported by the U.S. Department of Energy, OER-BES-DMS Grant No. DE-AC36-83-CH10093. The calculations were performed using the Cray T3E, located at the National Energy Research Scientific Computing Center which is supported by the Office of Energy Research of the U.S. Department of Energy.

APPENDIX: DESCRIPTION OF EMPIRICAL PSEUDOPOTENTIALS

In this Appendix we describe the empirical pseudopotential fits applied in this study. We use the notation NSO–EPM (SO–EPM) for pseudopotentials omitting (including) spin-orbit effects. In Tables II–VI the pseudopotential fits (EPM) are compared with the experimental data [37–64] and first-principles calculations (LAPW). Illustrated are band energies at high symmetry points (eV with respect to Γ_{15v}), the band-gap hydrostatic deformation potential $a_g(\Gamma)$, the valence band maximum hydrostatic deformation potential $a_v(\Gamma)$, biaxial deformation potential b, the electron effective mass m_e, and the heavy-hole effective mass (m_{hh}). Δ_0 denotes the spin-orbit splitting value. Table VII gives the calculated natural and strained valence band offsets. Table VIII gives the band-gap redshifts in CuPt ([111]-oriented SL with period $n5 1$) and $Z2$ ([001]-oriented SL with period $n5 2$) with respect to random alloy. Tables IX–XI list the pseudopotential parameters resulting from the fits.

*Electronic address: alex_zunger@nrel.gov

[1] A. Zunger and S. Mahajan, in *Handbook of Semiconductors*, (Elsevier, Amsterdam, 1994), Vol. 3B (see Sec. 4.3.1), p. 1399.

[2] A.G. Norman and G.R. Booker, J. Appl. Phys. **57**, 4715 (1985).

[3] T.L. McDevitt, S. Mahajan, D.E. Laughlin, W.A. Bonner, and V.G. Keramidas, Phys. Rev. B **45**, 6614 (1992).

[4] M. Tsuchiya, P.M. Petroff, and L.A. Coldren, Appl. Phys. Lett. **57**, 1690 (1989); M. Tsudriya, J.M. Gaines, R.H. Yan, R.J. Simes, P.O. Holtz, L.A. Coldren, and P.M. Petroff, Phys. Rev. Lett. **62**, 466 (1989).

[5] K. C. Hsieh, J. N. Baillargeon, and K. Y. Cheng, Appl. Phys. Lett. **57**, 2244 (1990).

[6] A. C. Chen, A. M. Moy, P. J. Pearah, K. C. Hsieh, and K. Y. Cheng, Appl. Phys. Lett. **62**, 1359 (1993).

[7] Y. Tang, H. T. Lin, D. H. Rich, P. Colter, and S. M. Vernon, Phys. Rev. B **53**, 10 501 (1996); D. H. Rich, Y. Tang, and H. T. Lin, J. Appl. Phys. **81**, 6837 (1997).

[8] A. Mascarenhas, R. G. Alonso, G. S. Horner, S. Froyen, K. C. Hsieh, and K. Y. Cheng, Superlattices Microstruct. **12**, 57 (1992).

[9] K. Y. Cheng, K. C. Hsieh, and J. N. Baillargeon, Appl. Phys. Lett. **60**, 2892 (1992).

[10] S. T. Chou, K. Y. Cheng, L. J. Chou and K. C. Hsieh, Appl. Phys. Lett. **66**, 2220 (1995).

[11] J. Mirecki Millunchick, R. D. Twesten, S. R. Lee, D. M. Follstaedt, E. D. Jones, S. P. Ahrenkiel, Y. Zhang, H. M. Cheong, and A. Mascarenhas, MRS Bull. **22**, 38 (1997).

[12] J. Mirecki Millunchick, R. D. Twesten, D. M. Follstaedt, S. R. Lee, E. D. Jones, Y. Zhang, S. P. Ahrenkiel, and A. Mascarenhas, Appl. Phys. Lett. **70**, 1402 (1997).

[13] J. Mirecki Millunchick, R. D. Twesten, S. R. Lee, D. M. Follstaedt, E. D. Jones, S. P. Ahrenkiel, Y. Zhang, H. M. Cheong, and A. Mascarenhas, J. Electron. Mater. **26**, 1048 (1997).

[14] T. Y. Seong, A. G. Norman, I. T. Ferguson, and G. R. Booker, J. Appl. Phys. **73**, 8227 (1993).

[15] S. W. Jun, T. Y. Seong, J. H. Lee, and B. Lee, Appl. Phys. Lett. **68**, 3443 (1996).

[16] S.-J. Kim, H. Asahi, M. Takemoto, K. Asami, M. Takeuchi, and S. Gonda, Jpn. J. Appl. Phys. **35**, 4225 (1996).

[17] J. Tersoff, C. Teichert, and M. G. Lagally, Phys. Rev. Lett. **76**, 1675 (1996).

[18] A. G. Norman, S. P. Ahrenkiel, H. Moutinho, M. M. Al-Jassim, A. Mascarenhas, J. Mirecki Millunchick, S. R. Lee, R. D. Twesten, D. M. Follstaedt, J. L. Reno, and E. D. Jones, Appl. Phys. Lett. **73**, 1844 (1998).

[19] B. J. Spencer, P. W. Voorhees, and S. H. Davis, Phys. Rev. Lett. **67**, 3696 (1991).

[20] J. Tersoff, Phys. Rev. Lett. **77**, 2017 (1996).

[21] I. P. Ipatovea, V. G. Malyshkin, A. A. Maradudlin, V. A. Shchukin, and R. F. Wallis, Phys. Rev. B **57**, 12 968 (1998).

[22] Y. Zhang and A. Mascarenhas, Phys. Rev. B **57**, 12 245 (1998).

[23]

[24] L.-W. Wang, L. Bellaiche, S.-H. Wei, and A. Zunger, Phys. Rev. Lett. **80**, 4725 (PC8 1 1 0 TDys